

Environmental carbonate chemistry selects for phenotype of recently isolated strains of *Emiliana huxleyi*

Rosalind E. M. Rickaby¹, Michaël Hermoso¹, Renee B. Y. Lee¹, Benjamin D. Rae^{1,2}, Ana M. C. Heureux¹, Cecilia Balestreri³, Leela Chakravarti³, Declan Schroeder³, Colin Brownlee³

¹ University of Oxford, Department of Earth Sciences, South Parks Road, Oxford OX1 3AN, UK

² ARC Centre of Excellence for Translational Photosynthesis, Division of Plant Sciences, Research School of Biology, The Australian National University, Canberra ACT 2601, Australia.

³ Marine Biological Association, Citadel Hill Laboratory, Plymouth PL1 2PB, UK

Abstract

Coccolithophorid algae, particularly *Emiliana huxleyi*, are prolific biomineralisers that, under many conditions, dominate communities of marine eukaryotic plankton. Their ability to photosynthesise and form calcified scales (coccoliths) has placed them in a unique position in the global carbon cycle. Contrasting reports have been made with regards to the response of *E. huxleyi* to ocean acidification. Therefore, there is a pressing need to further determine the fate of this key organism in a rising CO₂ world. In this paper, we investigate the phenotype of newly isolated, genetically diverse, strains of *E. huxleyi* from UK Ocean

Acidification Research Programme (UKOARP) cruises around the British Isles, the Arctic, and the Southern Ocean. We find a continuum of diversity amongst the physiological and photosynthetic parameters of different strains of *E. huxleyi* morphotype A under uniform, ambient conditions imposed in the laboratory. This physiology is best explained by adaptation to carbonate chemistry in the former habitat rather than being prescribed by genetic fingerprints such as the CMM motif. To a first order, the photosynthetic capacity of each strain is a function of both aqueous CO₂ availability, and calcification rate, suggestive of a link between carbon concentrating ability and calcification. The calcification rate of each strain is related to the natural environmental [CO₃²⁻] at the site of isolation, but some strains display low calcification rates at the highest [CO₃²⁻] when limited by low CO₂ availability and/or a lack of a carbon concentrating mechanism. The environmental selection revealed amongst our recently isolated strain collection points to the future outcompetition of the heavily calcified morphotypes B/C and R by more rapidly photosynthesising, and lightly calcified strains of morphotype A but with their rate of calcification highly dependent on the surface ocean saturation state.

Keywords: Coccolithophores; Carbonate chemistry; Photosynthesis; Calcification; Polysaccharides; Stable Isotopes

Phytoplankton culture, Photosynthesis, Coccoliths, Oxygen isotopes, Coccolith-associated polysaccharides

1. Introduction

Coccolithophores are the most abundant calcifying algae that inhabit our modern day oceans. Their innate ability to produce intricate, calcitic shells, the coccoliths has significant influence on the oceanic biological pump and hence, on the global carbon cycle (Sigman and Boyle, 2000; Hutchins, 2011). Therefore it is important to understand how a key biological species, like the present-day dominant *Emiliania huxleyi*, will respond to the anthropogenic rise in atmospheric CO₂ and more specifically to coeval ocean acidification.

It has become apparent that there is large intra-specific variation between *E. huxleyi* strains. Strain-specific variations in cell physiology, the ability to calcify and isotopic footprint may disagree with the treatment of this taxon as a homogenous group (Young et al., 2003; Langer et al., 2009; Mackinder et al., 2011). Recent work showed the existence of genetically diverse populations of *E. huxleyi* (Martinez et al., 2007, 2012; Bendif et al., 2014; Krueger-Hadfield et al., 2014). In addition, Iglesias-Rodriguez and co-workers (2006) uncovered high levels of genetic diversity in different *E. huxleyi* bloom events using microsatellite markers. This intraspecific genetic diversity of *E. huxleyi* was confirmed by comparative genomic analysis of 14 *E. huxleyi* strains; an analysis that described considerable diversity between their genomic sequences (Read et al. 2013). Unsurprisingly, this genetic variation is manifested in the form of morphological (high and low calcifying morphotypes; Young et al., 2003) and physiological diversity, as testified by the existence of distinct coccolith morphology motifs (CMMs) (e.g. Schroeder et al. 2005). This strain diversity is matched by a myriad of opposing responses observed in laboratory cultures that were subjected to a wide range of manipulations of their growing environment (Hoppe et al., 2011; Langer et al., 2009, Kottmeier et al., 2014; Sett et al., 2014).

Although laboratory cultures provide an important resource for investigating the biology of *E. huxleyi*, it is often argued that experiments using long-term laboratory cultures may instead document evolutionary adaptations to changes induced by the culture conditions (Lakeman et al. 2009; Lohbeck et al., 2012). This study is the first attempt to characterise the chemical (inorganic carbon) affinities, optima and physiologies of multiple strains of *E. huxleyi* recently isolated from broad geographical locations crossing gradients of carbonate chemistry and physical parameters. Our goal is to investigate whether genes or environmental controls influence morphotype and phenotype dominance; our working hypothesis being that spatial variation in ambient carbonate chemistry exerts a selection pressure on physiologically varied extant *E. huxleyi* morphotypes. Our study will enable predictions as to the likely morphotype succession, and impact on biogeochemistry, of a rising carbon availability scenario.

2. Methods

2.1. Strains

Strains of *E. huxleyi* were isolated from three recent research cruises. Monoclonal strains, D366 26-1, D366 36-2 and D366 80-4 were isolated in June/July 2011 on the RV *Discovery*, cruise number D366 that circumnavigated the British Isle as part of the UK Ocean Acidification programme (<http://www.surfaceoa.org.uk/>). Also part of that programme, ARC 27-1, ARC 39-1 and ARC 68-2 were isolated in June/July 2012 on the RRS *James Clark Ross*, cruise number JCR271, that started from Reykjavik, Iceland. The cruise map can be obtained from <http://www.arcticoacruise.org/>. Lastly, SO 14-2 and SO 21-2 were isolated from the Great Southern Coccolithophore Belt II initiative on the R/V Roger Revelle, cruise number RR1202, that took place on February/March 2012 and sailed from Durban, South

Africa to Freemantle, Australia. The location of each of the above strain can be found on Fig. 1 and in the Supplementary Table. We complemented our study with *E. huxleyi* RCC 1216 (from the Tasman Sea) and RCC 1256 (from the North Atlantic Ocean), both supplied by the Roscoff Culture Collection and maintained in laboratory conditions since 1998/1999. Alterations in PIC, POC, and growth rate of RCC1216 and RCC1256 in response to changing seawater carbonate chemistry have previously reported (Langer et al., 2009).

Environmental parameters (temperature, total alkalinity, concentration of dissolved inorganic carbon (DIC), and pH) for the *in situ* sampling location (Supplementary Table) were obtained from the British Oceanographic Data Centre. Environmental parameters for the strains collected during the Great Southern Coccolithophore Belt II initiative, and from the Roscoff Culture Collection were obtained from annual modern day temperatures, DIC, TA, salinity and pH for each site which were extracted from the World Ocean Atlas 2009 gridded 1° by 1° dataset (Antonov et al., 2010; Locarnini et al., 2010). In situ aqueous CO₂ and [CO₃²⁻] were computed via the software CO2CAL using salinity, temperature, total alkalinity and DIC (Robbins et al., 2010), using CO₂ constants from Mehrbach et al. (1973) refitted by Dickson and Millero (1987), KHSO₄ from (Dickson, 1990), using the seawater pH scale.

2.2. Laboratory culture of *E. huxleyi* strains

Emiliana huxleyi strains were cultured in aged natural seawater from the English Channel in closed 2.4 litre polycarbonate vessels. The medium was prefiltered (41 µm) and air-equilibrated by vigorous bubbling at 15 °C overnight. Prior to filter sterilisation (0.22 µm), the seawater was supplemented with minerals and metals as per Keller's K/2 medium (Keller et al., 1987), and vitamins as per Guillard's f/2 medium (Guillard and Ryther, 1962) and the pH corrected to pH 8.2 by addition of 1N NaOH. Under these conditions, the concentrations

of aqueous CO₂ in the culture media was around 11.5 μM kg_{sw}⁻¹. The cell cultures were maintained at 15 °C in 150 μmol photons m⁻² s⁻¹ PAR with a day:night photoperiod of 14:10 hours. Specific growth rates (μ) were obtained from measurements of cell density at very dilute concentrations using a Coulter Counter Z2 (Beckman-Coulter, USA) apparatus. Coccosphere and cell diameters were measured on the same apparatus fitted with a 50 μm aperture tube. For measurements of naked cell size, coccospheres were decalcified with 0.5 M HCl for 5 minutes.

Dilute semi-continuous batch cultures were maintained in order to reduce deviations from our desired carbonate chemistry, to avoid self-shading by cell cultures, and to prevent nutrient limitation. Briefly, we inoculated these cultures at an initial cell concentration of *ca* 50 cells mL⁻¹. When cell density reached *ca* 2500 cells per mL, the culture flasks were harvested and an aliquot subcultured into new medium, hence representing a semi-continuous culture strategy that was repeated up to five times for each bioassay (Hutchins et al., 2003).

2.3. Measurements of photosynthetic oxygen evolution and consumption

Photosynthetic oxygen evolution measurements were conducted largely as described previously (Rae et al., 2011, 2012), using a Clark-type oxygen electrode (Hansatech, UK) to monitor dissolved oxygen concentration. The oxygen electrode was two-point calibrated according to manufacturers instructions using air-equilibrated water and oxygen-free water prepared by bubbling with nitrogen.

An aliquot of dilute cell cultures was collected at hour two of the photoperiod at mid log-phase by centrifugation at 300-500 x g. Collected cells were gently resuspended in DIC-free assay medium [32 g L⁻¹ Instant Ocean salts (United Pet Group, Virginia, USA), 50 mM 4-(2-

hydroxyethyl)-1-piperazineethanesulfonic acid (HEPES)-NaOH, pH 8.2]. Cell counts were taken using an improved Neubauer haemocytometer, and chlorophyll *a* concentration was determined in 100% ethanol extracts of whole cells using spectrophotometric calculation constants for Phaeophytes (Ritchie, 2006). Absorbance measurements were made using a Lambda 650 Spectrophotometer (Perkin Elmer, USA).

Cell cultures were resuspended to 2.0 mg chlorophyll *a* mL⁻¹ in a final volume of 2.0 ml in the oxygen-electrode cuvette. The cells were allowed to deplete residual DIC from the assay buffer in sub-saturating light (*ca* 300 $\mu\text{mol photons m}^{-2} \text{ s}^{-1}$) to prevent photo-damage. Net photosynthetic oxygen evolution rates were measured as the rate of change of dissolved oxygen concentration as a function of dissolved DIC in saturating light (600 $\mu\text{mol photons m}^{-2} \text{ s}^{-1}$) by serial addition of known aliquots of NaHCO₃.

Respiration rates were recorded as oxygen consumption in the darkened cuvette prior to the first addition of NaHCO₃, and again after the final measurement. The ratio of the initial and final respiration values is reported here as “metabolic flexibility” and represents the ability of the cell culture to transiently increase metabolic rate in response to increased availability of DIC.

The photosynthetic rate constants $P_{\text{max}}^{\text{net}}$ and $P_{\text{max}}^{\text{gross}}$, representing maximum net and gross photosynthetic oxygen evolution respectively, and $K_{1/2}$ (DIC), representing the photosynthetic half-saturation constant for DIC, were interpolated from plots derived from this data (Fig. 2). $P_{\text{max}}^{\text{gross}}$ was calculated from the final respiration rate and $P_{\text{max}}^{\text{net}}$. Statistical analyses of triplicate measurements were calculated using Microsoft Excel (Microsoft, USA) and SPSS Statistics (IBM, USA). The photosynthetic half-saturation constant for DIC [$K_{1/2}$ (DIC)] was converted to $K_{1/2}$ (CO₂) using the CO2CALC program using the aforementioned parameters.

2.4. Polysaccharide extraction and measurement of UAC

The coccolith-associated polysaccharide (CAP) was extracted from cultured coccoliths using the protocol of Lee et al. (manuscript submitted). Harvested cells were cleaned with 1 % (v/v) Triton X-100 and 4.5 % (v/v) NaOCl in 0.05 M NaHCO₃. The coccolith pellet was resuspended 0.05 M NH₄HCO₃ by ultrasonication and further purified by centrifugation through a gradient of 100 mL Ludox TM-50 colloidal silica layered with 25 mL 20 % (w/v) sucrose at 23000 g for 20 min at 4 °C. Decalcification was carried out by incubating the pellet in 0.5M EDTA (pH 8.0) for 12 h. Insoluble residues were removed by centrifugation at 31000 g and the supernatant was diafiltered using an Amicon Ultracel membrane against 20 mM Tris-Cl (pH 8.0). Anion exchange liquid chromatography was carried out using a HiTrap DEAE FF column according to the manufacturer's protocol. The target polysaccharide was eluted with the same buffer containing 0.5 M NaCl. Finally, the CAP fraction was diafiltered against MilliQ. Total polysaccharide concentration was determined using a phenol-H₂SO₄ assay (Hodge and Hofreiter, 1962). The uronic acid content was determined with a modified carbazole-H₂SO₄ assay (Cesaretti et al., 2003) using a glucuronic acid standard. The values obtained were normalised to 4µg total polysaccharide. We obtained a low yield of polysaccharide for GS2 which raised a question as to the validity of its UAC results. CAPs were also subjected to 12% SDS-PAGE and stained with Alcian Blue according to Moller et al. (1993). The visualised bands on the denaturing PAGE gel were used to determine the relative mass of the strain-specific polysaccharides.

2.5. PIC/POC measurements and Calcification Rate

Approximately 3 mg of homogenised cell residue, rinsed with neutralised deionised water, were measured by oxidation / pyrolysis for their particulate inorganic carbon (PIC) and particulate organic carbon (POC) content using a Rock-Eval VI apparatus at the University of Oxford (see Hermoso et al., 2014 for details on the method). As the semi-continuous batch mode of culture did not permit generation of PIC/cell measurements, we have made estimates of bulk calcification rates for each strain. There are two potential ways to correct for the photosynthetic rate, by combining PIC/POC measurements with $\mu \times V$ assuming that the density of the organic matter was identical amongst cultured strains, or multiplying by P2000. Since one aim is to investigate how calcification rate varies with photosynthetic rates and capacity, we chose to use $\mu \times V$ as our correcting factor which maintains calcification as an independently derived measurement which is separate from our O₂ electrode measurements. With the assumption that cellular volume scales POC per cell within each strain being examined here, our rate of calcification was calculated as follows:

$$\text{Calcification Rate} = \text{cellular volume (V)} \times \mu \times \text{PIC/POC} \quad (\text{Eq. 1})$$

2.6. Scanning electron microscopy

Samples for scanning electron microscope (SEM) were filtered onto polycarbonate filters (2 μm pore size), rinsed with deionised water (pH 8.0), air-dried at room temperature for 24 hours, then sputter coated with gold-palladium. Imaging was carried out on a Jeol JSM-840A SEM at 20 kV.

Strains were assigned to morphotypes *sensu* Bown (1998,) and Young et al. (2003) by analysis of coccospheres and detached coccoliths using guidelines documented on the Nannotax3 website (<http://ina.tmsoc.org/Nannotax3/index.php?dir=Coccolithophores>)

(Table 1, Fig. 3). Coccosphere diameters between strains matched with measurement given by the Coulter Counter apparatus (Fig. 3). The presence of an organic matter coating on most specimens prevented statistically meaningful morphometric measurements for assessment of the degree of calcification, as established by Young et al. (2014) on natural specimens.

2.7. Isotopic measurements of coccolith calcite

The oxygen isotope ratios ($\delta^{18}\text{O}$) of the carbonate fraction of culture residues were measured using a VG Isogas Prism II mass spectrometer with an on-line VG Isocarb. Approximately 1 mg samples were rinsed to remove NaCl, subsequently cleaned using hydrogen peroxide (H_2O_2), and dried at 60 °C for at least 30 minutes. The carbonate was reacted with purified anhydrous phosphoric acid at 90°C within the instrument. Calibration to V-PDB (Vienna-PeeDee Belemnite) standard via NBS-19 is made daily using the Oxford in-house (NOCZ) Carrara marble standard. Reproducibility of replicated standards is usually better than 0.1 ‰ for $\delta^{18}\text{O}$.

3. Results of morphotype diversity

Our first order result is that diversity exists in physiological terms between morphotypes, but importantly within morphotype such that the nature of any one strain cannot capture the full range of the physiology possible within that morphotype.

3.1. Diverse specific growth rates amongst *E. huxleyi* strains

There is a relatively wide range of specific growth rates within the *E. huxleyi* strains subjected to the same culture conditions but having been isolated from a diversity of

temperature, light intensity, nutrient level, $[\text{CO}_2 \text{ aq}]$ and seawater pH (Fig. 1). Measured values range from 0.58 to 1.04 day^{-1} . Although there is a well established negative correlation between algal cell-size and growth rate, we observed no link between growth rate and cell size. Prior work has shown that algal growth rates are not exclusively determined by cell size, for instance species or strain-specific differences in nutrient limitation may play an important role in limiting growth (Kagami and Urabe, 2001). This is supported by biogeochemical modelling work (Tang, 1995; Aloisi, 2015). The only strain that operates less than one division per day ($< 0.69 \text{ day}^{-1}$), and corresponding to morphotype B/C, has the largest cellular volume. We observed a good relationship between cellular volume and coccosphere volume ($r^2 = 0.85$) (Table 1).

3.2 PIC/POC amongst *E. huxleyi* strains

Measured PIC/POC ratios reflect the bulk relative allocation of the internal carbon pool into coccolith calcite and organic matter by the cells over the course of the semi-continuous batch experiment. Overall, *E. huxleyi* has been documented as characterised by the lowest PIC/POC ratio compared to other common extant coccolithophore species that may contribute to their relative ecological success in modern oceanic settings (Langer et al., 2009; Gerech et al., 2014; Hermoso et al., 2014). Here, we demonstrate that significant differences exist across strains from values of 2.74 to 0.51 under conditions of 2000 $\mu\text{mol/kg}$. Our two Southern Ocean strains (SO1 and SO2) display the highest values, a PIC/POC > 2 , which is higher than the PIC/POC often reported for *Coccolithus braarudii* and *Gephyrocapsa oceanica*, each considered as species which prioritise calcification more highly than *E. huxleyi* (e.g. Rickaby et al., 2010; Gerech et al., 2014). Similarly the lowest PIC/POC of 0.51 from the NIS strain under ambient conditions is amongst the lowest reported.

3.3 Photosynthetic Rates

For the same availability of carbon, the diverse strains achieve a range of different physiologies and photosynthetic rates. Considerable variation was observed between the maximum rates of net photosynthetic oxygen evolution (P_{\max}^{net}). These ranged from 26.3 ± 0.5 fmol O₂ cell⁻¹ h⁻¹ (strain IC) to 99.6 ± 4.6 fmol O₂ cell⁻¹ h⁻¹ (strain NS1). When the influence of basal respiration rate was taken into account, a similar magnitude of difference was observed in the gross photosynthetic oxygen evolution rates (P_{\max}^{gross}): 35.6 ± 3.3 to 121.7 ± 8.6 fmol O₂ cell⁻¹ h⁻¹ (same strains). The P_{\max}^{net} reported for TS/RCC1216 (28.5 ± 4.1 fmol O₂ cell⁻¹ h⁻¹) compares favourably to previously reported values under substantially similar conditions – *c.f.* 26 ± 6 fmol O₂ cell⁻¹ h⁻¹ (Rokitta and Rost, 2012). The photosynthetic rates at near ambient environmental conditions of 2000 $\mu\text{mol kg}^{-1}$ DIC (P_{2000}) also vary almost by an order of magnitude, increasing seven-fold from NIS, TS and IC through NS1, GS2 to BB, SO1, SO2 with the greatest P_{2000} in NS2, GS1.

We have two approaches to assessing the photosynthetic efficiency of each strain. Our measure of P_{2000} , and a photosynthetic carbon fixation index as per Bidigare et al. (1997) (Eq. 2):

$$\text{Photosynthetic carbon fixation index} = \text{cellular volume} \times \text{growth rate} \quad (\text{Eq. 2})$$

It might be expected that P_{2000} should generally scale with our measured cell size and growth rate: the greater the photosynthetic rate (P_{2000}) (Fig. 4 or Table 1), the larger the cell and the greater the division rate. Although linear relationships do exist between P_{2000} and

photosynthetic fixation ($\mu \times V$), two distinct groups appear amongst our strains (Fig. 4). Some strains (e.g. NS1 and GS2) achieve a greater cell size and growth rate for the same P_{2000} than e.g. SO1, SO2 and BB. For others, e.g. NS2 and GS 1, they achieve equivalent growth rates and cell size to GS2 and NS1 but at much higher photosynthetic rates. P_{2000} is an incontrovertible measure of the photosynthetic rate, the rate of CO_2 fixation into organic carbon under ambient conditions. But $\mu \times V$ (an approximation for the realised cellular output from photosynthetic carbon fixation), must be considered alongside the additional cellular output of calcification. For the energy budget provided by P_{2000} , different strains apportion more energy towards μ and V (e.g. NS2, NS1) while others prioritise calcification (SO1, SO2) at the expense of their growth rate and/or volume. Similarly different strains may use alternative strategies to achieve P_{2000} . P_{2000} likely increases with CO_2 availability in the internal pool, and the amount of enzyme (D-Ribulose-1,5-Bisphosphate carboxylase/oxygenase (RuBisCO)) available for photosynthesis such that a high P_{2000} may be reached via a concentrated internal pool or a high availability of RubisCO (more discussion below).

3.4 CAP Results

Biominalisation in coccolithophores is regulated by several components, namely acidic polysaccharides and the organic base plate (Westbroek et al., 1973). *E. huxleyi* has been shown to possess only one acidic polysaccharide (Kayano & Shiraiwa 2009) but further work by Borman et al. (1982, 1987) uncovered a diversity in the CAPs across strains of *E. huxleyi* which, they suggest, may influence the rate of calcite precipitation. Our results concur with Borman et al. (1982, 1987), whereby a diversity in both the CAP mass (Fig. 5) and uronic acid content (UAC), the carboxylated monosaccharide likely to chelate calcium, (Table 1)

was observed. The monosaccharide composition of polysaccharides influence its interaction with a variety of compounds, including calcium carbonate. *In vitro* studies have demonstrated that the chemical make-up, particularly the level of carboxyl and sulfated groups in polysaccharides can control the degree and rate of calcite nucleation (e.g. Borman et al. 1982). We find that the UAC is markedly different between morphotypes, with NIS morphotype B/C exhibiting a lower UAC at 0.93, compared to the heavily calcified TS morphotype R (UAC = 2.71), whilst a surprisingly wide range of UAC, from 1.15 to 2.57, was recorded across less calcified coccoliths assigned to morphotype A strains.

4. Discussion of Selection of Phenotype by the Environment

Of utmost interest in the context of ocean acidification, is how elevated carbon availability will affect the distribution and success of prevalent calcifiers such as *E. huxleyi*. In the modern ocean, there is some logic in the distribution of the different morphotypes of *E. huxleyi*, which may owe to the saturation state of calcite in the mixed-layer (Bach et al., 2011; Borchard et al., 2011). This newly isolated strain collection from the UK Ocean Acidification Program of cruises offers a unique opportunity to investigate the natural selection for strains of contrasting physiologies, representative of the conditions at the site of isolation, by gradients in environmental carbon system parameters. In the following, we will try to characterise the intracellular carbon dynamics of individual morphotypes and ascribe them to their inherent adaptation to carbon availability in the environment. Inter-strain variation was observed for all types of data presented in this study, and this variation probably has its root in the genetic and genomic variability observed amongst *E. huxleyi* strains (Read et al., 2013). Nonetheless we find no rationalisation of the different physiologies by their CMM motif. Instead the strongest physiological signal relates strains to

preserving an inherent adaptation to environmental chemistry at the site of isolation. Although we shall discuss IC and TS in the same context as all the other strains, we must add a note of caution that these strains have been maintained in culture for two decades and are most susceptible therefore to artefact. Nonetheless, by and large their physiology also can be rationalised by the environment at their sites of selection suggestive that the genetic differences are strongly conserved and resistant to decay despite their maintenance for greater than a decade in artificial conditions.

4.1 Selection of physiology by environmental carbonate chemistry

We find the most apparent correlation between the aqueous CO₂ availability at the site of strain collection, exponentially with the P_{\max} of different strains (linear regression on $\ln(P_{\max})$ with aqueous CO₂ yields $R^2 = 0.56$ and p-value < 0.05, Fig. 6). Such a relationship between *E. huxleyi* physiology and dissolved CO₂ availability seems reasonable since this species has been documented to rely on a diffusive supply of CO₂ for 80-90% of its carbon assimilation under “normal” ambient DIC conditions (Kottmeier et al., 2014; Holtz et al., 2015). This potential maximum photosynthetic rate appears to be the most robust physiological identifier of the different strains and dictates many of the derived parameters from the oxygen electrode, such as $K_{1/2}^{\text{CO}_2}$ (a notional inorganic carbon affinity of the cell) and P_{2000} (photosynthetic CO₂ fixation rate under ambient conditions) which both show a strong correlation with P_{\max} , increasing in value as P_{\max} increases (Fig. 4, and Fig. 6; Table 1). It may be that P_{\max} is a physiological characteristic most resistant to adaptive change during the interim period of culture maintenance since environmental isolation.

But how can a “potential” photosynthetic rate be a factor under selection by the real ambient environment at the site of strain isolation? P_{\max} is the CO₂-saturated photosynthetic rate, and the maximum electron-transport rate viable for a given cell, in some sense the photosynthetic capacity of the cell. All else being equal (i.e. nutrient availability), one of the dominant factors underpinning P_{\max} is the total RuBisCO content of the cell, i.e. the enzyme responsible for the photosynthetic fixation of CO₂. At saturating inorganic-carbon, the photosynthetic rate is controlled by the abundance of RuBisCO, the CO₂ concentration in the cellular compartment containing RuBisCO, and the rate of production of energy equivalents by light-dependent reactions of photosynthesis. Due in part to inefficient discrimination for CO₂ and poor enzymatic rate by RuBisCO, this enzyme is required in large quantities in *E. huxleyi*; RuBisCO is thus the most nitrogen intensive sink for the cell. It is likely therefore, that the character of the strains that is preserved, is the cellular concentration of RuBisCO. High P_{\max} values seem largely to be driven by the CO₂ availability in the environment from which each strain was isolated (Fig. 5); it stands to reason that the cells are able to invest more resources to achieve higher photosynthetic rates when CO₂ is more abundant.

It is intuitive to any observer that, if physiological variability in *E. huxleyi* is selected by the environment and influences the locally dominant strain, that *E. huxleyi* be somewhat stable in its phenotype over the time frame on which local DIC conditions vary. That is to say, the culture acclimation time of *E. huxleyi* exceeds the time frame on which they have been in culture. Moreover, in cell culture, the *mode* of selection remains, i.e. environmental parameters of cell culture will apply a selective pressure to the population of cells. However, the *effect* of selection is lost, i.e. the selection pressure no longer leads to subspecies succession due to a loss of fitness. Taken together, we reason that *E. huxleyi* cells in long or

short term culture might begin to phenotypically adapt to their conditions, but they do not suffer a fitness cost; particularly when repeatedly subcultured into very low density cultures.

There are two very distinct outliers from this general increase in P_{\max} with CO_2 , which lie at the extrema of CO_2 availability for our strain collection: GS1 which has an apparently very low P_{\max} for its CO_2 availability, and SO2, which has a very high P_{\max} for its CO_2 availability. Across the range of physiological parameters measured, these two outliers in terms of P_{\max} also stand out for their cellular PIC/POC ratio with GS1 having the lowest PIC/POC of 0.51, and SO2 the highest value of 2.74. P_{\max} therefore appears to covary with both CO_2 availability, and with our derived parameter for the cellular calcification rate (Fig. 6b). At steady state the cellular input of carbon equals the cellular output. So this relationship between P_{\max} and calcification rate could reflect that the higher the photosynthetic turnover for the cell, the greater the output of carbon to calcification. Nonetheless, to rationalise the carbon input, P_{\max} cannot depend on CO_2 alone. Alleviation of a limiting factor, be it a nutrient or light, acts to elevate P_{\max} . So the dependence of P_{\max} on both CO_2 availability, and on rates of calcification bolsters suspicions that calcification could be acting as a carbon concentrating mechanism (CCM) and an additional source of CO_2 fuelling photosynthesis (Buitenhuis et al., 1999). This additional CO_2 source could allow for a greater investment in RuBisCO (when environmental CO_2 is very low) thus elevating the P_{\max} of the highly calcifying strains (e.g. SO2). Alternatively, it could imply that these strains invoking higher calcification rates also express a CCM to facilitate the higher carbon flux associated with high calcification rates. Nonetheless a linkage between calcification and CCM is controversial (Leonardos et al., 2009; Bach et al., 2013).

P_{\max} appears to be the most pristine physiological (and genetic) coded signal of the environmental conditions at the site of isolation and is best conserved since the transition to the culture maintenance conditions. The P_{\max} reveals that the strains with the greater photosynthetic capacity, and indeed carbon requirement in terms of cell size, growth rate and calcification, are selected for by a higher availability of dissolved aqueous CO_2 . Alternatively, cells with a greater requirement for carbon are successful in higher carbon environments, but there is a confounding factor: calcification, which potentially boosts, or correlates with an alternative physiological mechanism which also elevates photosynthetic rates for equivalent CO_2 availability.

4.2 What controls calcification of the *E. huxleyi* population?

To a first order both calcification and realised photosynthetic rates (P_{2000}) increase with CO_2 availability at the strain isolation sites suggestive that an increasing diffusive CO_2 supply selects strains with higher rates of photosynthesis and calcification, but two outliers to the relationship emerge again: GS1 and SO2 with highest and lowest calcification rates at the respective extrema of CO_2 availability (Fig 7a). The more apparent control on the calcification rate of the strains, is environmental CO_3^{2-} at the isolation sites, with higher calcification rates linearly related to higher carbonate ion concentrations/saturation state (Fig. 7b). There are three exceptions to this relationship: IC, TS and BB each of which have a low calcification rate but were isolated from sites with some of the highest CO_3^{2-} concentrations of our strain collection ($>200 \mu\text{mol/kg}$). Due to the inherent constraints of the carbonate system, an inverse relationship exists between the $[\text{CO}_3^{2-}]$ and CO_2 in the waters such that high $[\text{CO}_3^{2-}]$ waters also have low CO_2 , as seawater pH remains relatively constant. The ambient $[\text{CO}_3^{2-}]/\text{CO}_2$ ratio for these strains with a low PIC/POC is greater than 11. The only

other strain isolated from waters with similar chemistry was SO2 which achieves a much higher calcification rate but as we shall detail below, is suspected of possessing a CCM to facilitate such high calcification rates. The most reasonable explanation for the low calcification rates of TS and IC, despite the high $[\text{CO}_3^{2-}]$, is that these cells are limited by the CO_2 supply rate as evidenced by their lowest growth rate and cellular volume (Fig. 4b), and have little to no carbon concentrating capability (discussed below). These two strains were also isolated two decades ago. BB is somewhat anomalous in that the CO_2 availability for this strain does not appear to be limiting. We note, however, that BB was isolated from a subtropical latitude, a zone where phytoplankton are susceptible to other forms of limitation e.g. by nutrients or light if deeper dwelling.

The striking linear correlation between our laboratory derived estimates of calcification rate, and the $[\text{CO}_3^{2-}]$ at the site of isolation provides evidence for the constitutive expression of the calcification rate whilst under culture conditions at least in the short term. It also shows the selection by the CO_3^{2-} concentration for the more highly calcifying strains, as also suggested by Beaufort et al. (2011), where CO_2 is sufficient to allow the expression of calcification at that level. Mechanistically, this dependence of calcification rate on external $[\text{CO}_3^{2-}]$ at the site of isolation could be explained by increased ease of H^+ expulsion at high $[\text{CO}_3^{2-}]$ (Bach et al., 2015; Hermoso, 2015). We note that extrapolation of this linear correlation between calcification rate and $[\text{CO}_3^{2-}]$, to a calcification rate of zero suggests that morphotype A calcification could cease at a $[\text{CO}_3^{2-}]$ of approximately 80 $\mu\text{mol/kg}$, even with high CO_2 availability.

4.3 Presence or absence of a CCM

It has been hypothesised that elevating CO₂, would allow for a fertilisation and redistribution of energy due to a relaxed need for the expression of a CCM required at low CO₂ availability (Badger et al., 1998; Hopkinson et al., 2011; Raven et al., 2014). Therefore documenting the relative expression of a CCM within these recently isolated strains is important to understand whether relaxed CCM requirements under elevated CO₂ availability, could contribute to increased success of certain strains amongst these different *E. huxleyi* morphotypes. *Emiliana huxleyi*, as a species, is often assumed to lack CCM expression at ambient conditions, relying dominantly on diffusive supply of CO₂ (Kottmeier et al., 2014; Holtz et al., 2015).

4.3.1 Absence of a CCM from $K_{1/2}^{CO_2}$

We are able to assess the presence of a CCM across our strains by comparing the cellular $K_{1/2}^{CO_2}$ to the K_m of RuBisCO and to the environmental CO₂ availability. $K_{1/2}^{CO_2}$ is the external CO₂ concentration required to half-saturate photosynthetic oxygen evolution. This cellular kinetic value represents the totality of the cellular response to external DIC, and incorporates the enzyme affinities of potential membrane transporters for DIC, the action of internal and external carbonic anhydrase (CA) enzymes, the magnitude of the DIC pools in various cellular compartments, and the specific kinetics of this primary carbon-fixing enzyme, RuBisCO.

This $K_{1/2}^{CO_2}$ value can be compared to the enzymatic half-saturation constant for CO₂ ($K_M^{CO_2}$) for the RuBisCO enzyme (Badger et al., 1998). Here the $K_{1/2}^{CO_2}$ value varied over a sizeable range. The strains with the highest affinity for CO₂ possessed $K_{1/2}^{CO_2}$ values in the 10-20 μ M range (strains NS2, BB, SO1, SO2, and IC). These values are well below the 40 - 77 μ M

$K_M^{CO_2}$ value reported for the *E. huxleyi* RuBisCO enzyme (Young and Heureux pers. comm.; Boller et al., 2011). Although we cannot rule out interstrain variation in RuBisCO kinetics, all strains except TS and NIS exhibited a significantly higher affinity for CO_2 than the documented concomitant RuBisCO kinetics under our acclimation conditions. Since the affinity of the cell for CO_2 is higher than that of the photosynthetic enzyme, this might suggest that all strains possess an active CCM to some extent, apart from TS and NIS. But such an interpretation may be confounded in calcifiers like coccolithophores due to the dual destination of carbon for photosynthesis and calcification. Calcifiers will have a higher affinity for carbon than their RuBisCO merely because they require carbon for two purposes so that in cells with a PIC/POC of 1, a cellular $K_{1/2}^{CO_2}$ half of that of the $K_M^{CO_2}$ of RuBisCO would satisfy the RuBisCO and calcification demand rather than reflecting the workings of a CCM.

The exceptionally high $K_{1/2}^{CO_2}$ values of TS and NIS are indicative of very low carbon affinity. These strains also have a low maximum photosynthetic rate (P_{max}), and low calcification rate suggesting a lack of any CCM presence. We know from previous work that TS is almost entirely dependent on a passive diffusive supply of CO_2 for photosynthesis at pH 8.2 (Kottmeier et al., 2014), so it is not surprising that we observe low photosynthetic rates, and poor cellular kinetics. Of note is that TS and NIS which lack a CCM, operate at a PIC/POC of ~ 1 which induces no net change of intracellular pH or carbonate chemistry, assuming no loss of H^+ from the cell. By contrast, the lower CO_2 selected morphotype A strains generate a PIC/POC $\gg 1$, whereby the high calcification rates yield net pH lowering or CO_2 , each of which could be harnessed to enhance CO_2 acquisition for photosynthesis.

The ratio of $K_{1/2}^{CO_2}/CO_2(aq)$ provides an alternative indicator of whether the carbon requirement of a strain is satisfied by CO_2 availability in the environment, or could require additional HCO_3^- to function. From this perspective, GS1 is carbon replete with a ratio < 1 , BB, NS2, SO1, GS2 and IC range from 0.88 to 1.3 and so are approximately matched by the environmental availability of CO_2 such that no additional HCO_3^- uptake is apparently required. By contrast NS1, NIS and TS have values significantly higher than 1 (1.5 to 6.8) suggestive that the environment is carbon deficient for those strains consistent with a lack of CCM in NIS and TS. At face value, NS1 may seek additional carbon input from HCO_3^- but the $K_{1/2}^{CO_2}$ may be elevated by the high P_{max} of this strain and high calcification rate.

4.3.2 Presence of a CCM from oxygen isotopes in coccolith calcite

The $\delta^{18}O$ of the coccolith calcite also allows some insight into the carbon source and dynamics of the internal pool and calcification. The oxygen isotope composition of *E. huxleyi* coccolith calcite is consistently shifted towards positive values with respect to equilibrium conditions. Despite the chemically instantaneous transformation of CO_2 to HCO_3^- (at $pH \sim 7$; Anning et al., 1996), the ionic forms of DIC transiently maintain a heavy $\delta^{18}O$ signature inherited from the source of carbon, which for *E. huxleyi* is CO_2 . Taking the oxygen isotope system as a whole, oxygen atoms of water in seawater and even in the cytoplasm represent an infinite reservoir compared to the tiny fraction of oxygen present in CO_2 and HCO_3^- . After CO_2 assimilation by the cell and conversion into HCO_3^- imposed by pH conditions, the oxygen atoms borne by the DIC and water will continue to isotopically exchange and as a result, the heavy isotopic signature of the DIC species will diminish as equilibration takes place. In solution, the time required to (re)-equilibrate the oxygen isotope of the H_2O – DIC system is of the order of 12 hours at 15 °C (Usdowski et al., 1991; Zeebe and Wolf-Gladrow, 2001; Zeebe, 2009). So the magnitude of a heavy oxygen isotopic vital effect reflects the

residence time of carbon within the cell before calcification and the persistence of a heavy isotopic signature, insufficient time for equilibration with the abundant H₂O (Hermoso, 2014; Hermoso et al., 2014; 2015).

As our experiments were performed at constant temperature and constant $\delta^{18}\text{O}_{\text{sw}}$, observed $\delta^{18}\text{O}$ differences between strains are representative of physiological variability. A relatively wide range of $\delta^{18}\text{O}$ composition is measured between strains from +0.94 to +2.70‰ with an average of +2.07 ‰ (Table 1). We note that morphotypes B/C and R have oxygen isotope compositions indistinguishable from morphotypes A and that no correlation exists between cell size and $\delta^{18}\text{O}$.

In our experiments, most strains are offset from inorganic conditions (calculated at +0.43 ‰ VPDB according to the experiments by Kim and O’Neil, 1997). The maximum offset (vital effect) is as high as ~ 2.0 ‰ (Fig. 8). The preservation of oxygen isotopic disequilibria illustrates the speed of the mineralisation of the internal carbon pool allocated to calcification, compared to other species such as *C. pelagicus* that typically precipitates calcite at near-equilibrium conditions (Rickaby et al., 2010; Stevenson et al., 2014; Hermoso, 2015). Four strains stand out from the generally isotopically heavy group as being closer to equilibrium: NS 1, NS 2, SO1 and SO2 (Fig. 8). These strains partly eliminate this isotopically “heavy signal” (sensu Dudley et al., 1986). In contrast to the prevailing view that these strains should have the slowest calcification rates that allow sufficient time for CO₂ isotopic equilibration with H₂O, these strains are characterised by the fastest calcification rates, and high overall internal DIC pool turnover rates (Fig. 8). There are two possible explanations for these apparently contradictory results. These strains (NS 1, NS 2, SO1 and SO2) could either induce a coccolith vesicle carbonic anhydrase to support their high calcification rates, which

accelerates the isotopic equilibration between CO_2 and H_2O (Uchikawa and Zeebe, 2012; Watkins et al., 2013). Alternatively they are able to induce uptake of HCO_3^- under the ambient conditions. As HCO_3^- has a significantly lower $\delta^{18}\text{O}$ with respect to CO_2 (Zeebe and Wolf-Gladrow, 2001), that some strains are closer to equilibrium can indeed be explained by a higher $\text{HCO}_3^-/\text{CO}_2$ supply. This feature has been recently found to represent a response to alleviate carbon limitation by *E. huxleyi* cells (Kottmeier et al., 2014, Sett et al., 2014). Each of these considerations represents some cellular investment by NS 1, NS 2, SO1 and SO2 in carbon management above mere reliance on diffusive supply of CO_2 . Given the dependence of P_{max} on calcification however it could imply that these strains prioritise investment in e.g. a carbonic anhydrase to elevate calcification as a means of supplementing their photosynthetic rates.

4.3.3 A measure of intracellular carbon: Characterisation of coccolith-associated polysaccharides (CAPs)

A recent study has hypothesised that coccolithophores regulate the UAC in accordance with the amount of carbon available within the internal pool (Lee et al., submitted). Here, we establish a direct relationship between the UAC of each strain CAP to the size of the internal carbon pool, as proxied by P_{2000}/P_{max} (Fig. 9), with the exception of TS and GS2. We have suggested that P_{2000} is a function of both internal CO_2 , and the concentration of cellular RuBisCO. This concentration of RuBisCO is most likely proportional to P_{max} such that P_{2000} is a function of $P_{\text{max}} \times \text{CO}_2$ (Fig. 9b) assuming that the cells are still acclimated to their environmental CO_2 , and that diffusion is the dominant mechanism supplying the internal pool. Therefore the UAC can be compared to P_{2000}/P_{max} as a proxy for the amount of carbon in the internal pool. NS2 and GS1 exhibiting the highest UAC, have the greatest P_{2000} and the

highest inferred internal carbon pool. In contrast, the low UAC of NIS is associated with a low photosynthetic rate and small internal carbon pool. We note that NIS (morphotype B/C) seems to be at one extreme of the continuum of the morphotype A and does not sit distinctly from that trend. TS stands apart from the group, either because it is a distinct morphotype (R) or because it has an exceptionally small internal carbon pool. We have no explanation for the exceptionally high UAC content of GS2 apart from the methodological reservations due to low yield expressed in section 2.4.

Amongst the morphotype A strains, the UAC acts as an estimate for the charge density of CAP. The more charged CAPs correlate with a higher availability of internal carbon pool. Although this suggestion may seem counter-intuitive (since a more highly charged molecule is perceived to be more efficient at attracting ions for nucleation at a lower supersaturation), Giuffrè *et al.* (2013) have shown that substrates poorer in carboxyl functional groups actually promote the fastest nucleation rates at lower supersaturation since more polar substrates bind more competitively with water molecules under these conditions. Therefore calcite nucleation is more efficient at lower degrees of supersaturation mediated by lesser charged molecules (low UAC), and faster at higher degrees of supersaturation mediated by more polar molecules (high UAC).

5. Summary and the fate of *E. huxleyi* morphotypes in a higher carbon future ocean.

We show that no one strain can characterise the breadth of physiology displayed by a single morphotype but instead, different strains represent a continuum of physiological selection across environmental gradients. Our evidence from the archive of environmental adaptation preserved in the physiology of recently isolated strains, suggests that in a future higher CO₂

world, the low CO₂-adapted morphotype B/C and R will be marginalised and, without adaptation, may eventually be outcompeted. Elevated CO₂ will instead select for the higher-CO₂ adapted morphotype As, with a resultant faster rate of carbon fixation but declining calcification rate. Amongst the morphotype As, we find a strong relationship between the photosynthetic capacity of different strains and their calcification rate, at all CO₂ availabilities, which is suggestive that calcification is linked to photosynthesis by enhancing the carbon supply for photosynthesis and alleviating a limitation on P_{\max} , perhaps by increasing the generation of RuBisCO. Calcification rates of our strains show a strong linear dependence on [CO₃²⁻], even suggesting that strains, with no further adaptation, may no longer calcify at a [CO₃²⁻] of < 80 µmol/kg. Elevating CO₂ and reducing CO₃²⁻ naturally reduces this fertilising effect of calcification on photosynthesis.

Acknowledgements

We are grateful to the NERC UKOA Sea Surface Consortium grant number NE/H017119/1, and the ERC grant SP2-GA-2008-200915 for funding. We are also indebted to the Master and crew of the RV *Discovery*, cruise number D366, RRS *James Clark Ross*, cruise number JCR271, and the R/V Roger Revelle, cruise number RR1202 for support during each of the cruises. We thank Harry McClelland for discussions about statistics and isotopes, Ian Probert for scientific insight, and Chris Day for assistance in isotopic analyses.

References

Aloisi, G., 2015. Co-variation of metabolic rates and cell-size in coccolithophores.

Biogeosciences Discuss. 12, 6215–6284. doi:10.5194/bgd-12-6215-2015

652 Antonov, J.I., et al, 2010. World Ocean Atlas 2009 (Volume 2: Salinity). Report. Washinton
 653 D.C.

654 Bach, L.T., Riebesell, U., Schulz, K.G., 2011. Distinguishing between the effects of ocean
 655 acidification and ocean carbonation in the coccolithophore *Emiliana huxleyi*. Limnol.
 656 Oceanogr. 56, 2040–2050. doi:10.4319/lo.2011.56.6.2040.

657 Bach, L.T., Mackinder, L.C.M., Schulz, K.G., Wheeler, G., Schroeder, D.C., Brownlee, C.,
 658 Riebesell, U., 2013. Dissecting the impact of CO₂ and pH on the mechanisms of
 659 photosynthesis and calcification in the coccolithophore *Emiliana huxleyi*. New Phytol.
 660 199, 121–34. doi:10.1111/nph.12225

661 Bach, L.T., Riebesell, U., Gutowska, M.A., Federwisch, L., Schulz, K.G., 2015. A unifying
 662 concept of coccolithophore sensitivity to changing carbonate chemistry embedded in an
 663 ecological framework. Prog. Oceanogr. 135, 125–138.
 664 doi:10.1016/j.pocean.2015.04.012

665 Badger, M.R., Andrews, T.J., Whitney, S.M., Ludwig, M., Yellowlees, D.C., Leggat, W.,
 666 Price, G.D., 1998. The diversity and coevolution of Rubisco, plastids, pyrenoids, and
 667 chloroplast-based CO₂-concentrating mechanisms in algae. Can. J. Bot. 76, 1052–1071.
 668 doi:10.1139/b98-074.

669 Beaufort, L., Probert, I., de Garidel-Thoron, T., Bendif, E.M., Ruiz-Pino, D., Metzl, N.,
 670 Goyet, C., Buchet, N., Coupel, P., Grelaud, M., Rost, B., Rickaby, R.E.M., de Vargas,
 671 C., 2011. Sensitivity of coccolithophores to carbonate chemistry and ocean acidification.
 672 Nature 476, 80–3. doi:10.1038/nature10295

673 Bidigare, R.R., Fluegge, A., Freeman, K.H., Hanson, K.L., Hayes, J.M., Hollander, D.,
 674 Jasper, J.P., King, L.L., Laws, E.A., Milder, J., Millero, F.J., Pancost, R., Popp, B.N.,
 675 Steinberg, P.A., Wakeham, S.G., 1997. Consistent fractionation of ¹³C in nature and in
 676 the laboratory: Growth-rate effects in some haptophyte algae. Global Biogeochem.

677 Cycles 11, 279–292. doi:10.1029/96GB03939

678 Boller, A.J., Thomas, P.J., Cavanaugh, C.M., Scott, K.M., 2011. Low stable carbon isotope
679 fractionation by coccolithophore RubisCO. *Geochim. Cosmochim. Acta* 75, 7200–7207.
680 doi:10.1016/j.gca.2011.08.031

681 Borchard, C., Borges, A. V., Händel, N., Engel, A., 2011. Biogeochemical response of
682 *Emiliana huxleyi* (PML B92/11) to elevated CO₂ and temperature under phosphorous
683 limitation: A chemostat study. *J. Exp. Mar. Bio. Ecol.* 410, 61–71.
684 doi:10.1016/j.jembe.2011.10.004

685 Borman, A.H., de Jong, E.W., Huizinga, M., Kok, D.J., Westbroek, P., Bosch, L., 1982. The
686 role in CaCO₃ crystallization of an acid Ca²⁺-binding polysaccharide associated with
687 coccoliths of *Emiliana huxleyi*. *Eur. J. Biochem.* 129, 179–83.

688 Borman, A.H., Jong, E.W., Thierry, R., Westbroek, P., Bosch, L., Gruter, M., Kamerling,
689 J.P., 1987. Coccolith-associated polysaccharides from cells of *Emiliana huxleyi*
690 (Haptophyceae). *J. Phycol.* 23, 118–123. doi:10.1111/j.1529-8817.1987.tb04433.x

691 Bown, P., 1998. *Calcareous Nannofossil Biostratigraphy*. Kluwer Academic.

692 Buitenhuis, E.T., de Baar, H.J.W., Veldhuis, M.J.W., 1999. Photosynthesis and calcification
693 by *Emiliana huxleyi* (Prymnesiophyceae) as a function of inorganic carbon species. *J.*
694 *Phycol.* 35, 949–959. doi:10.1046/j.1529-8817.1999.3550949.x

695 Cesaretti, M., Luppi, E., Maccari, F., Volpi, N., 2003. A 96-well assay for uronic acid
696 carbazole reaction. *Carbohydr. Polym.* 54, 59–61. doi:10.1016/S0144-8617(03)00144-9

697 Dickson, A.G., 1990. Standard potential of the reaction $\text{AgCl(s)} + .5\text{H}_2\text{(g)} = \text{Ag(s)} + \text{HCl(aq)}$
698 and the standard acidity constant of the ion HSO_4^- in synthetic sea water from 273.15 to
699 318.15 K. *J. Chem. Thermodynamics.* 22, 113–127.

700 Dickson, A.G., Millero, F.J., 1987. A comparison of the equilibrium constants for the
701 dissociation of carbonic acid in seawater media. *Deep Sea Res. Part A. Oceanogr. Res.*

702 Pap. 34, 1733–1743. doi:10.1016/0198-0149(87)90021-5
 703 Dudley, W., Blackwelder, P., Brand, L., Duplessy, J.-C., 1986. Stable isotopic composition of
 704 coccoliths. *Mar. Micropaleontol.* 10, 1–8.
 705 Giuffre, A.J., Hamm, L.M., Han, N., Yoreo, J.J. De, Dove, P.M., De Yoreo, J.J., 2013.
 706 Polysaccharide chemistry regulates kinetics of calcite nucleation through competition of
 707 interfacial energies. *Proc. Natl. Acad. Sci. U. S. A.* 110, 9261–6.
 708 doi:10.1073/pnas.1222162110
 709 Guillard, R.R.L., Ryther, J.H., 1962. Studies of marine planktonic diatoms: i. *Cyclotella* Nana
 710 hustedt, and *Detonula Confervacea* (Cleve) Gran. *Can. J. Microbiol.* 8, 229–239.
 711 doi:10.1139/m62-029
 712 Hermoso, M., 2014. Coccolith-derived isotopic proxies in palaeoceanography: where
 713 geologists need biologists. *Cryptogam. Algal.* 35, 323–351.
 714 doi:10.7872/crya.v35.iss4.2014.323
 715 Hermoso, M., Horner, T.J., Minoletti, F., Rickaby, R.E.M., 2014. Constraints on the vital
 716 effect in coccolithophore and dinoflagellate calcite by oxygen isotopic modification of
 717 seawater. *Geochim. Cosmochim. Acta* 44, 612–627. doi:10.1016/j.gca.2014.05.002
 718 Hermoso, M., 2015. Control of ambient pH on growth and stable isotopes in phytoplanktonic
 719 calcifying algae. *Paleoceanography* 30. doi:10.1002/2015PA002844
 720 Hermoso, M., Candelier, Y., Browning, T.J., Minoletti, F., 2015. Environmental control of
 721 the isotopic composition of subfossil coccolith calcite: Are laboratory culture data
 722 transferable to the natural environment? *GeoResJ* 7, 35–42.
 723 doi:10.1016/j.grj.2015.05.002
 724 Hodge, J.E., Hofreiter B.T., 1962. Determination of reducing sugar and carbohydrates.
 725 *Methods in Carbohydrate Chemistry*, Vol. 1., eds Whistler RL, Wolfrom ML, BeMiller
 726 J.N., Shafizadeh, F., Academic Press, New York, pp 380-394.

727 Holtz, L.-M., Wolf-Gladrow, D., Thoms, S., 2015. Numerical cell model investigating
 728 cellular carbon fluxes in *Emiliana huxleyi*. J. Theor. Biol. 364, 305–15.
 729 doi:10.1016/j.jtbi.2014.08.040
 730 Hopkinson, B.M., Dupont, C.L., Allen, A.E., Morel, F.M.M., 2011. Efficiency of the CO₂-
 731 concentrating mechanism of diatoms. Proc. Natl. Acad. Sci. U. S. A. 108, 3830–7.
 732 doi:10.1073/pnas.1018062108
 733 Hoppe, C.J.M., Langer, G., Rost, B., 2011. *Emiliana huxleyi* shows identical responses to
 734 elevated pCO₂ in TA and DIC manipulations. J. Exp. Mar. Bio. Ecol. 406, 54–62.
 735 doi:10.1016/j.jembe.2011.06.008
 736 Hutchins, D.A., 2011. Oceanography: Forecasting the rain ratio. Nature 476, 41–2.
 737 doi:10.1038/476041a
 738 Hutchins, D.A., Pustizzi, F., Hare, C.E., DiTullio, G.R., 2003. A shipboard natural
 739 community continuous culture system for ecologically relevant low-level nutrient
 740 enrichment experiments. Limnol. Oceanogr. Methods 1, 82–91.
 741 doi:10.4319/lom.2003.1.82
 742 Iglesias-Rodríguez, M.D., Probert, I., Batley, J., 2006. Microsatellite cross-amplification in
 743 coccolithophores: application in population diversity studies. Hereditas 143, 99–102.
 744 doi:10.1111/j.2006.0018-0661.01933.x
 745 Kagami, M., Urabe, J., 2001. Phytoplankton growth rate as a function of cell size: An
 746 experimental test in Lake Biwa. Limnology 2, 111–117.
 747 Keller, M.D., Selvin, R.C., Claus, W., Guillard, R.R.L., 2007. Media for the culture of
 748 oceanic ultraphytoplankton. J. Phycol. 23, 633–638. doi:10.1111/j.1529-
 749 8817.1987.tb04217.x
 750 Kim, S.-T., O’Neil, J.R., 1997. Equilibrium and nonequilibrium oxygen isotope effects in
 751 synthetic carbonates. Geochim. Cosmochim. Acta 61, 3461–3475. doi:10.1016/S0016-

7037(97)00169-5

Kottmeier, D.M., Rokitta, S.D., Tortell, P.D., Rost, B., 2014. Strong shift from HCO₃⁻ to CO₂ uptake in *Emiliana huxleyi* with acidification: new approach unravels acclimation versus short-term pH effects. *Photosynth. Res.* doi:10.1007/s11120-014-9984-9

Krueger-Hadfield, S.A., Balestreri, C., Schroeder, J., Highfield, A., Helaouët, P., Allum, J., Moate, R., Lohbeck, K.T., Miller, P.I., Riebesell, U., Reusch, T.B.H., Rickaby, R.E.M., Young, J., Hallegraeff, G., Brownlee, C., Schroeder, D.C., 2014. Genotyping an *Emiliana huxleyi* (prymnesiophyceae) bloom event in the North Sea reveals evidence of asexual reproduction. *Biogeosciences* 11, 5215–5234. doi:10.5194/bg-11-5215-2014

Lakeman, M.B., von Dassow, P., Cattolico, R.A., 2009. The strain concept in phytoplankton ecology. *Harmful Algae* 8, 746–758. doi:10.1016/j.hal.2008.11.011

Langer, G., Nehrke, G., Probert, I., Ly, J., Ziveri, P., 2009. Strain-specific responses of *Emiliana huxleyi* to changing seawater carbonate chemistry. *Biogeosciences* 6, 2637–2646. doi:10.5194/bg-6-2637-2009

Leonardos, N., Read, B., Thake, B., Young, J.R., 2009. No mechanistic dependence of photosynthesis on calcification in the coccolithophorid *Emiliana huxleyi* (Haptophyta). *J. Phycol.* 45, 1046–1051. doi:10.1111/j.1529-8817.2009.00726.x

Lee, R.B., Mavridou, D.A.I., Papadakos, G., McClelland, H.L.O.M., Rickaby, R.E.M. Lifting the CAP on biomineralization in coccolithophores. Submitted.

Locarnini, R., et al., 2010. World Ocean Atlas 2009 (Volume 1: Temperature). Report. Washington D.C.

Lohbeck, K.T., Riebesell, U., Reusch, T.B.H., 2012. Adaptive evolution of a key phytoplankton species to ocean acidification. *Nat. Geosci.* 5, 346–351. doi:10.1038/ngeo1441

Mackinder, L., Wheeler, G., Schroeder, D., von Dassow, P., Riebesell, U., Brownlee, C.,

777 2011. Expression of biomineralization-related ion transport genes in *Emiliana huxleyi*.
 778 Environ. Microbiol. 13, 3250–65. doi:10.1111/j.1462-2920.2011.02561.x
 779 Martínez, J.M., Schroeder, D.C., Larsen, A., Bratbak, G., Wilson, W.H., 2007. Molecular
 780 dynamics of *Emiliana huxleyi* and cooccurring viruses during two separate mesocosm
 781 studies. Appl. Environ. Microbiol. 73, 554–62. doi:10.1128/AEM.00864-06
 782 Martínez, J.M., Schroeder, D.C., Wilson, W.H., 2012. Dynamics and genotypic composition
 783 of *Emiliana huxleyi* and their co-occurring viruses during a coccolithophore bloom in
 784 the North Sea. FEMS Microbiol. Ecol. 81, 315–23. doi:10.1111/j.1574-
 785 6941.2012.01349.x
 786 Mehrbach, C., Culberson, C.H., Hawley, J.E., Pytkowicz, R.M., 1973. Measurement of the
 787 apparent dissociation constants of carbonic acid in seawater at atmospheric pressure.
 788 Limnol. Oceanogr. 18, 897–907. doi:10.4319/lo.1973.18.6.0897
 789 Møller, H.J., Heinegård, D., Poulsen, J.H., 1993. Combined alcian blue and silver staining of
 790 subnanogram quantities of proteoglycans and glycosaminoglycans in sodium dodecyl
 791 sulfate-polyacrylamide gels. Anal. Biochem. 209, 169–75. doi:10.1006/abio.1993.1098
 792 Rae, B.D., Förster, B., Badger, M.R., Price, G.D., 2011. The CO₂-concentrating mechanism
 793 of *Synechococcus* WH5701 is composed of native and horizontally-acquired
 794 components. Photosynth. Res. 109, 59–72. doi:10.1007/s11120-011-9641-5
 795 Rae, B.D., Long, B.M., Badger, M.R., Price, G.D., 2012. Structural determinants of the outer
 796 shell of β -carboxysomes in *Synechococcus elongatus* PCC 7942: roles for CcmK2, K3-
 797 K4, CcmO, and CcmL. PLoS One 7, e43871. doi:10.1371/journal.pone.0043871
 798 Raven, J.A., Beardall, J., Giordano, M., 2014. Energy costs of carbon dioxide concentrating
 799 mechanisms in aquatic organisms. Photosynth. Res. 121, 111–24. doi:10.1007/s11120-
 800 013-9962-7
 801 Read, B.A., Kegel, J., Klute, M.J., Kuo, A., Lefebvre, S.C., Maumus, F., Mayer, C., Miller,

802 J., Monier, A., Salamov, A., Young, J., Aguilar, M., Claverie, J.-M., Frickenhaus, S.,
 803 Gonzalez, K., Herman, E.K., Lin, Y.-C., Napier, J., Ogata, H., Sarno, A.F., Shmutz, J.,
 804 Schroeder, D., de Vargas, C., Verret, F., von Dassow, P., Valentin, K., Van de Peer, Y.,
 805 Wheeler, G., Dacks, J.B., Delwiche, C.F., Dyhrman, S.T., Glöckner, G., John, U.,
 806 Richards, T., Worden, A.Z., Zhang, X., Grigoriev, I. V, 2013. Pan genome of the
 807 phytoplankton *Emiliana* underpins its global distribution. *Nature* 499, 209–13.
 808 doi:10.1038/nature12221

809 Rickaby, R.E.M., Henderiks, J., Young, J.N., 2010. Perturbing phytoplankton: response and
 810 isotopic fractionation with changing carbonate chemistry in two coccolithophore
 811 species. *Clim. Past* 6, 771–785. doi:10.5194/cp-6-771-2010

812 Ritchie, R.J., 2006. Consistent sets of spectrophotometric chlorophyll equations for acetone,
 813 methanol and ethanol solvents. *Photosynth. Res.* 89, 27–41. doi:10.1007/s11120-006-
 814 9065-9

815 Robbins, L.L., Hansen, M.E., Kleypas, J.A., Meylan, S.C., 2010. CO2calc—A user-friendly
 816 seawater carbon calculator for Windows, Max OS X, and iOS (iPhone). U.S. Geol. Surv.
 817 - File Report.

818 Schroeder, D., Biggi, G., Hall, M., Davy, J., Martinez, J., Richardson, A., Malin, G., Wilson,
 819 W., 2005. A genetic marker to separate *Emiliana huxleyi* (Prymnesiophyceae)
 820 morphotypes. *J. Phycol.* 41, 874–879. doi:10.1111/j.1529-8817.2005.000100.x

821 Sett, S., Bach, L.T., Schulz, K.G., Koch-Klavsen, S., Lebrato, M., Riebesell, U., 2014.
 822 Temperature Modulates Coccolithophorid Sensitivity of Growth, Photosynthesis and
 823 Calcification to Increasing Seawater pCO₂. *PLoS One* 9, e88308.
 824 doi:10.1371/journal.pone.0088308

825 Sigman, D.M., Boyle, E.A., 2000. Glacial/interglacial variations in atmospheric carbon
 826 dioxide. *Nature* 407, 859–869.

827 Stevenson, E.I., Hermoso, M., Rickaby, R.E.M., Tyler, J.J., Minoletti, F., Parkinson, I.J.,
 828 Mokadem, F., Burton, K.W., 2014. Controls on Stable strontium isotope fractionation in
 829 coccolithophores with implications for the marine Sr cycle. *Geochim. Cosmochim. Acta*
 830 128, 225–235. doi:10.1016/j.gca.2013.11.043
 831 Tang, E.P.Y., 1995. The allometry of algal growth rates. *J. Plankton Res.* 17, 1325–1335.
 832 doi:10.1093/plankt/17.6.1325
 833 Uchikawa, J., Zeebe, R.E., 2012. The effect of carbonic anhydrase on the kinetics and
 834 equilibrium of the oxygen isotope exchange in the CO₂–H₂O system: Implications for
 835 $\delta^{18}\text{O}$ vital effects in biogenic carbonates. *Geochim. Cosmochim. Acta* 95, 15–34.
 836 doi:10.1016/j.gca.2012.07.022
 837 Usdowsli, E., Michaelis, J., Böttcher, M.E., Hoefs, J., 1991. Factors for the oxygen isotope
 838 equilibrium fractionation between aqueous and gaseous CO₂, carbonic acid,
 839 bicarbonate, carbonate, and water (19°C). *Z. Phys. Chem.* 170, 237–249.
 840 Watkins, J.M., Nielsen, L.C., Ryerson, F.J., DePaolo, D.J., 2013. The influence of kinetics on
 841 the oxygen isotope composition of calcium carbonate. *Earth Planet. Sci. Lett.* 375, 349–
 842 360. doi:10.1016/j.epsl.2013.05.054
 843 Westbroek, P., Jong, E.W., Dam, W., Bosch, L., 1973. Soluble intracrystalline
 844 polysaccharides from coccoliths of *Coccolithus huxleyi* (Lohmann) kamptner (I). *Calcif.*
 845 *Tissue Res.* 12, 227–238. doi:10.1007/BF02013737
 846 Young, J., Geisen, M., Cros, L., Kleijne, A., Sprengel, C., Probert, I., Ostergaard, J.B., 2003.
 847 A guide to extant coccolithophore taxonomy. *J. Nanoplankt. Res. Spec. Issue* 1, 1–125.
 848 Young, J.R., Poulton, A.J., Tyrrell, T., 2014. Morphology of *Emiliania huxleyi* coccoliths on
 849 the northwestern European shelf – is there an influence of carbonate chemistry?
 850 *Biogeosciences* 11, 4771–4782. doi:10.5194/bg-11-4771-2014
 851 Zeebe, R.E., 2009. Hydration in solution is critical for stable oxygen isotope fractionation

between carbonate ion and water. *Geochim. Cosmochim. Acta* 73, 5283–5291.

doi:10.1016/j.gca.2009.06.013

Zeebe, R.E., Wolf-Gladrow, 2001. *CO₂ in Seawater: Equilibrium, Kinetics, Isotopes*.

Elsevier.

Figure Captions:

Figure 1: Map showing mean annual aqueous CO₂ concentrations from the World Ocean Atlas dataset 2013 and the sampling locations of examined *E. huxleyi* strains. The map was generated using Ocean Data View (<http://odv.awi.de>). Where the sampling was not covered by the WOA dataset, we have annotated the dissolved aqueous CO₂ concentrations measured *in situ* at the sampling location. We reiterate that all measurements used in following figures and tables are *in situ* measurements taken from the cruise at the time of sampling, apart from SO1 and SO2.

Figure 2: A typical A/Ci curve, representing the photosynthetic oxygen evolution in response to external CO₂ concentration.

Figure 3: SEM images of coccospheres from the different strains of *Emiliania huxleyi* used in this study. A) NS1, B) NS2, C) BB, D) SO1, E) GS1, F) GS2, and G) NIS. All strains are morphotype A, with the exception of NIS (morphotype B/C) and TS (morphotype R).

Figure 4: a) A/Ci curves for our different *E. huxleyi* morphotypes/strains: NS1 (filled circles), NS2 (filled squares), BB (half-filled squares), SO1 (open right-angle triangle), SO2 (filled

right-angle triangle), GS1 (down-pointing filled triangle), GS2 (up-pointing filled triangle), NIS (open square), TS (open circle), IC (down-pointing open triangle); and b) The rate of photosynthetic evolution of O_2 in $mmol/h/10^6$ cells) at $2000 \mu mol/kg$ DIC versus our measured growth rate (μ) \times volume (V).

Figure 5: Denaturing polyacrylamide gel electrophoresis (SDS-PAGE). In all, $4\mu g$ coccolith-associated polysaccharide (CAP) was subjected to 12% SDS-PAGE and stained with Alcian Blue.

Figure 6: a) The relationship between maximum (P_{max} , black) rate of photosynthetic evolution of O_2 in $mmol/h/10^6$ cells) and that at $2000 \mu mol/kg$ DIC (P_{2000} , grey) versus the environmental aqueous CO_2 at the site of strain isolation derived from in situ measurement apart from SO1 and SO2 which derived from GLODAP for the different strains: NS1 (filled circles), NS2 (filled squares), BB (half-filled squares), SO1 (open right-angle triangle), SO2 (filled right-angle triangle), GS1 (down-pointing filled triangle), GS2 (up-pointing filled triangle), NIS (open square), TS (open circle), IC (down-pointing open triangle); b) The correlation between P_{max} and Calcification rate derived from $V \times \mu \times PIC/POC$ using the same symbols as above.

Figure 7: a) Lack of coherent correlation across the entire range of Aqueous CO_2 and PIC/POC (black) or Calcification rate derived from $V \times \mu \times PIC/POC$ compared to b) the significant relationship between Calcification rate derived from $V \times \mu \times PIC/POC$ and CO_3^{2-} from the site of isolation ($R^2 = 0.82$ for the linear relationship excluding the three outliers).

Figure 8: Oxygen isotope composition of the coccoliths (in ‰ V-PDB) versus calcification rate derived from $V \times \mu \times \text{PIC/POC}$. The dashed line represents the average 2.0 ‰ offset to heavier values, for the majority of strains, than calculated equilibrium at our culture conditions of 0.43 ‰ which is equivalent to the x-axis horizon of the plot, apart from strains SO2, NS2, SO1 and NS1

Figure 9: a) Uronic Acid Content of extracted coccolith associated polysaccharide (CAP) versus an estimate of the intracellular carbon concentration in the form of P_{2000}/P_{max} . b) P_{2000} as a function of $P_{\text{max}} \times \text{Aqueous CO}_2$ to demonstrate that the photosynthetic rate is a function of intracellular CO_2 , assuming a close relationship to extracellular CO_2 , and RuBisCO content.

Table 1. The range of physiological parameters recorded from the various strains and morphotypes of *Emiliania huxleyi* grown at ambient CO_2 (2000 $\mu\text{mol/kg DIC}$).

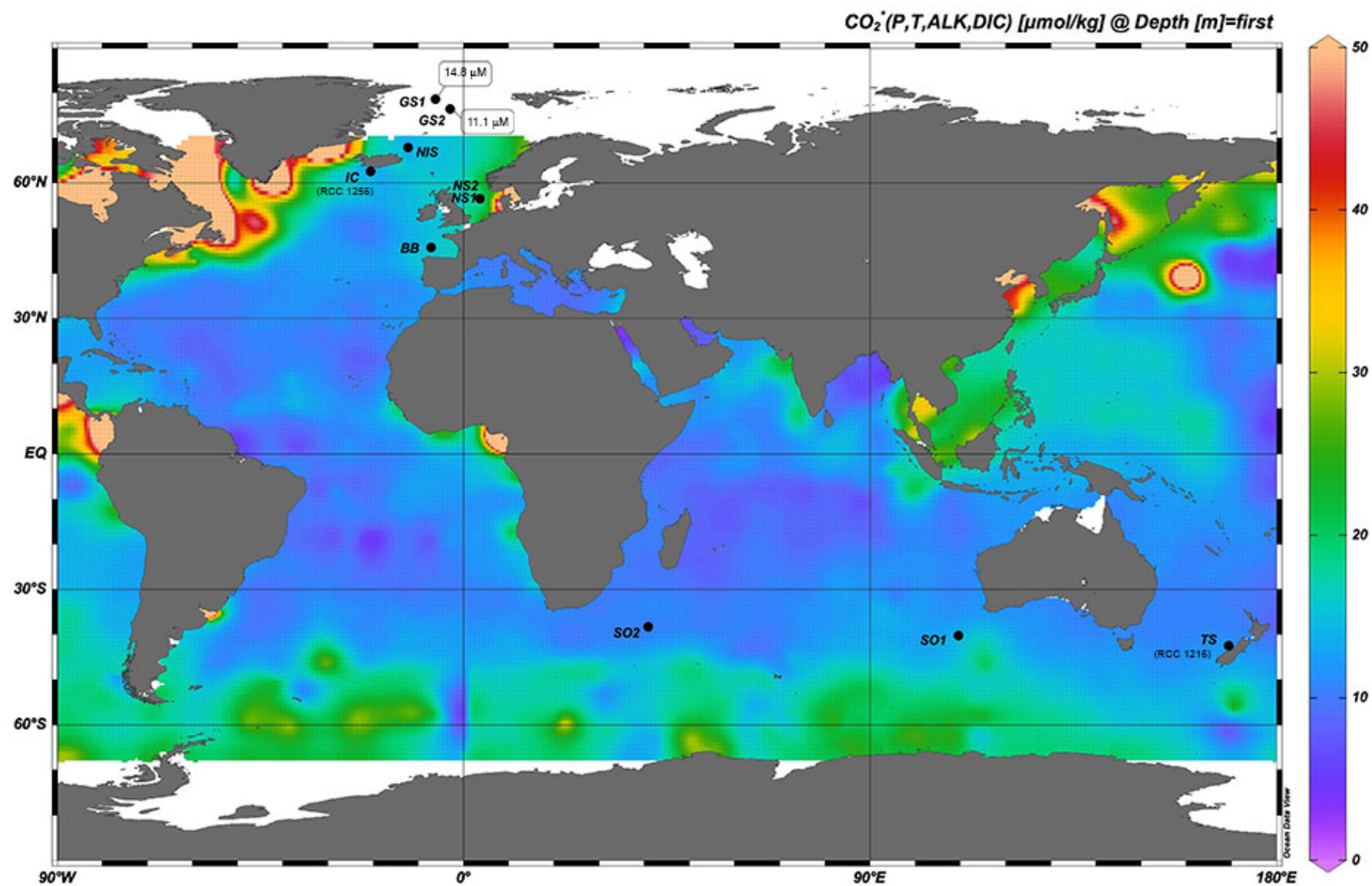


Fig. 1

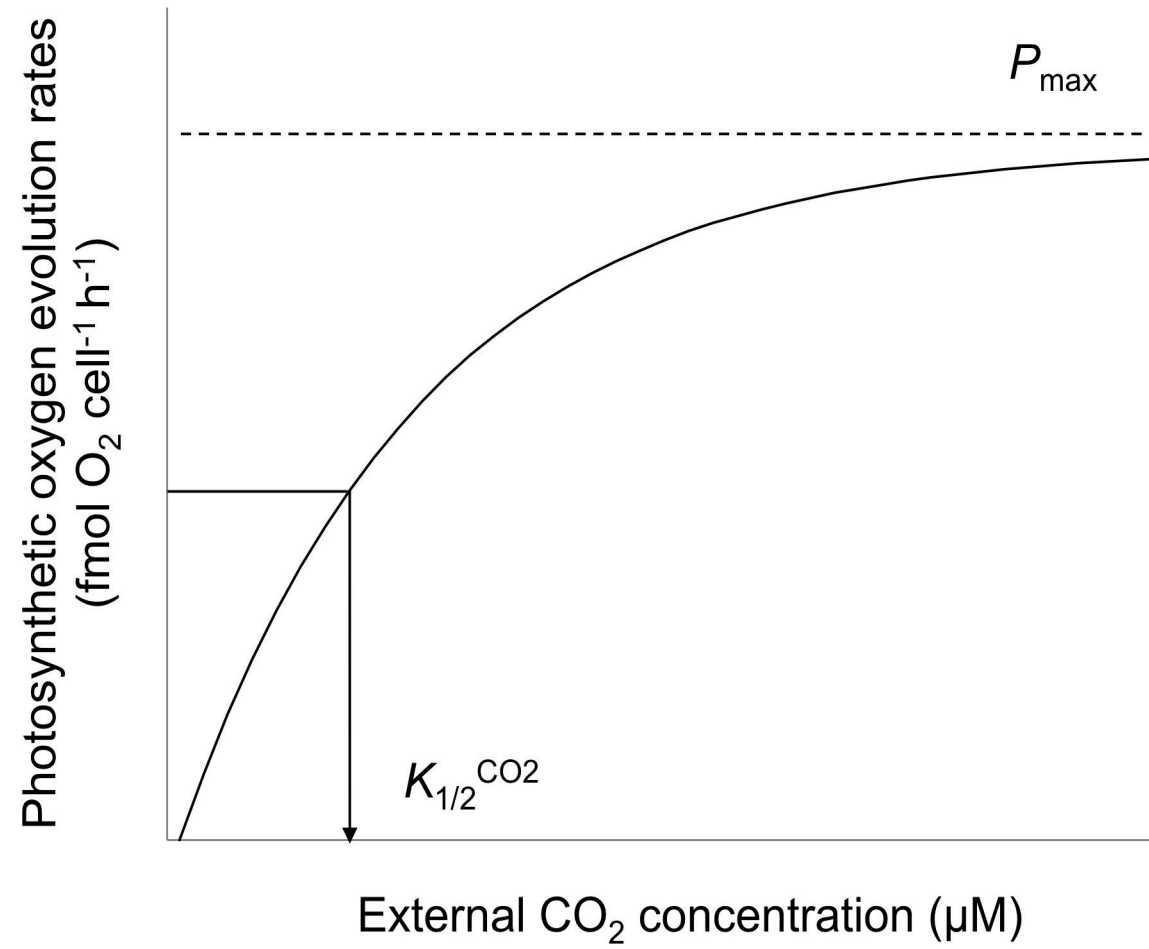


Fig. 2

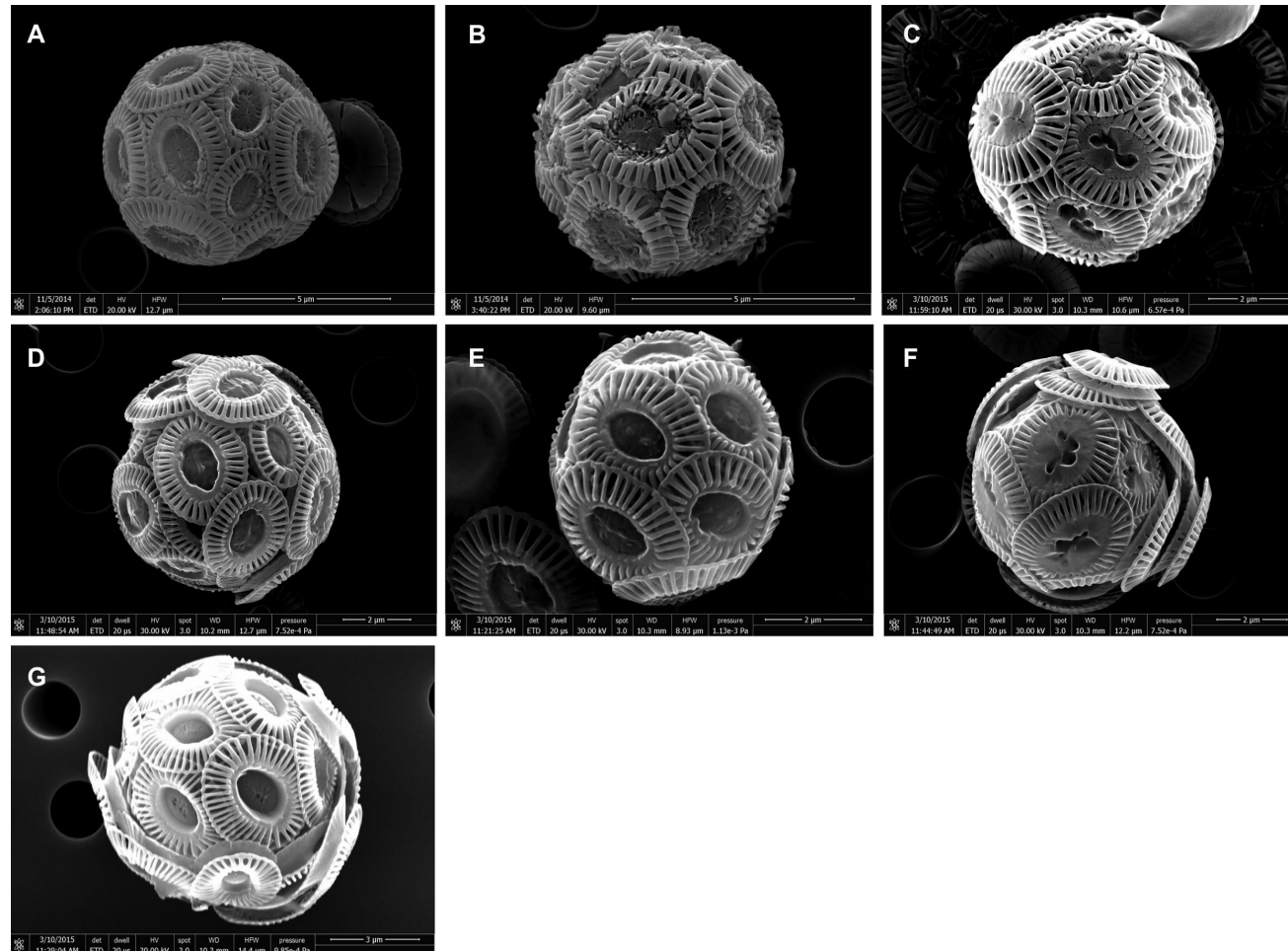


Fig. 3

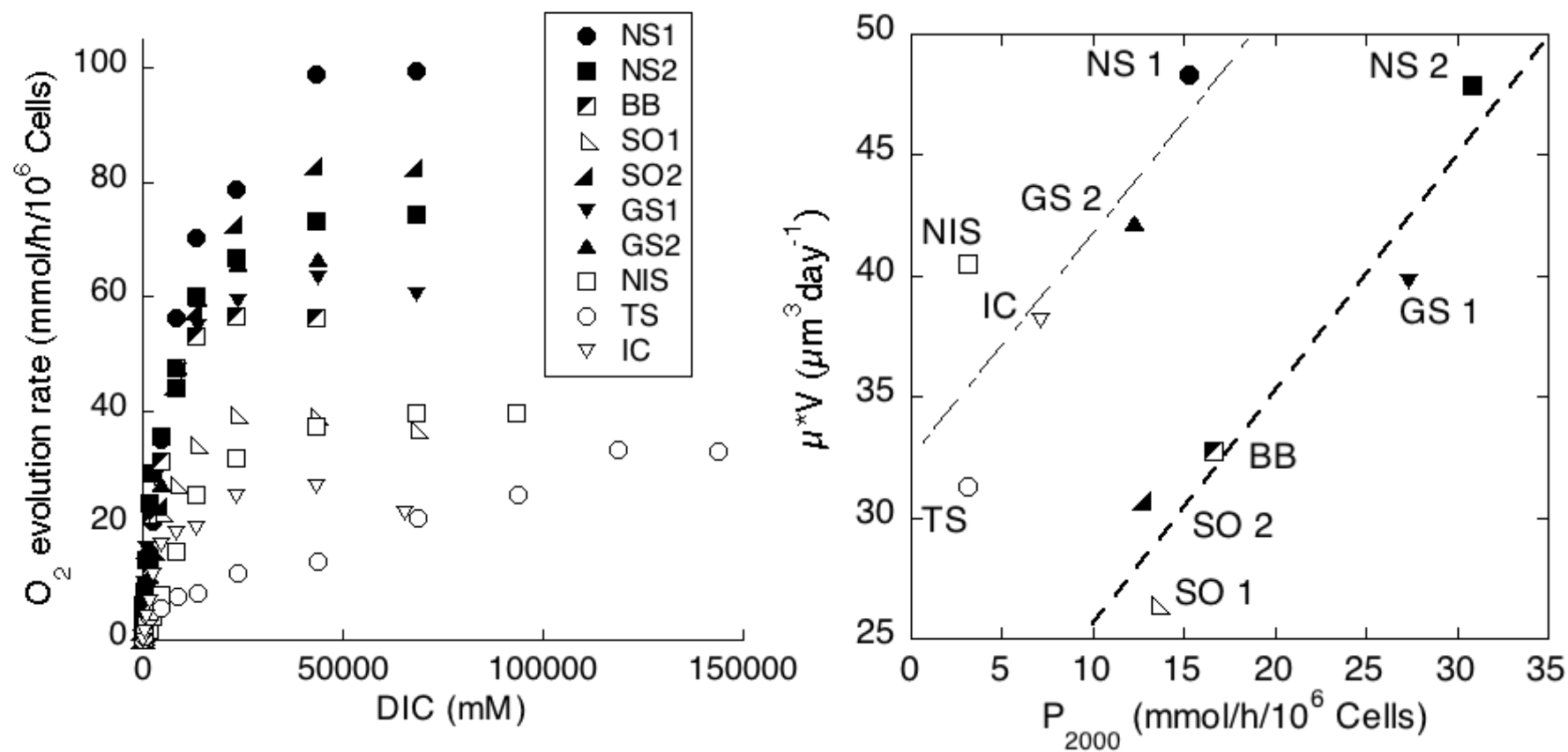


Fig. 4

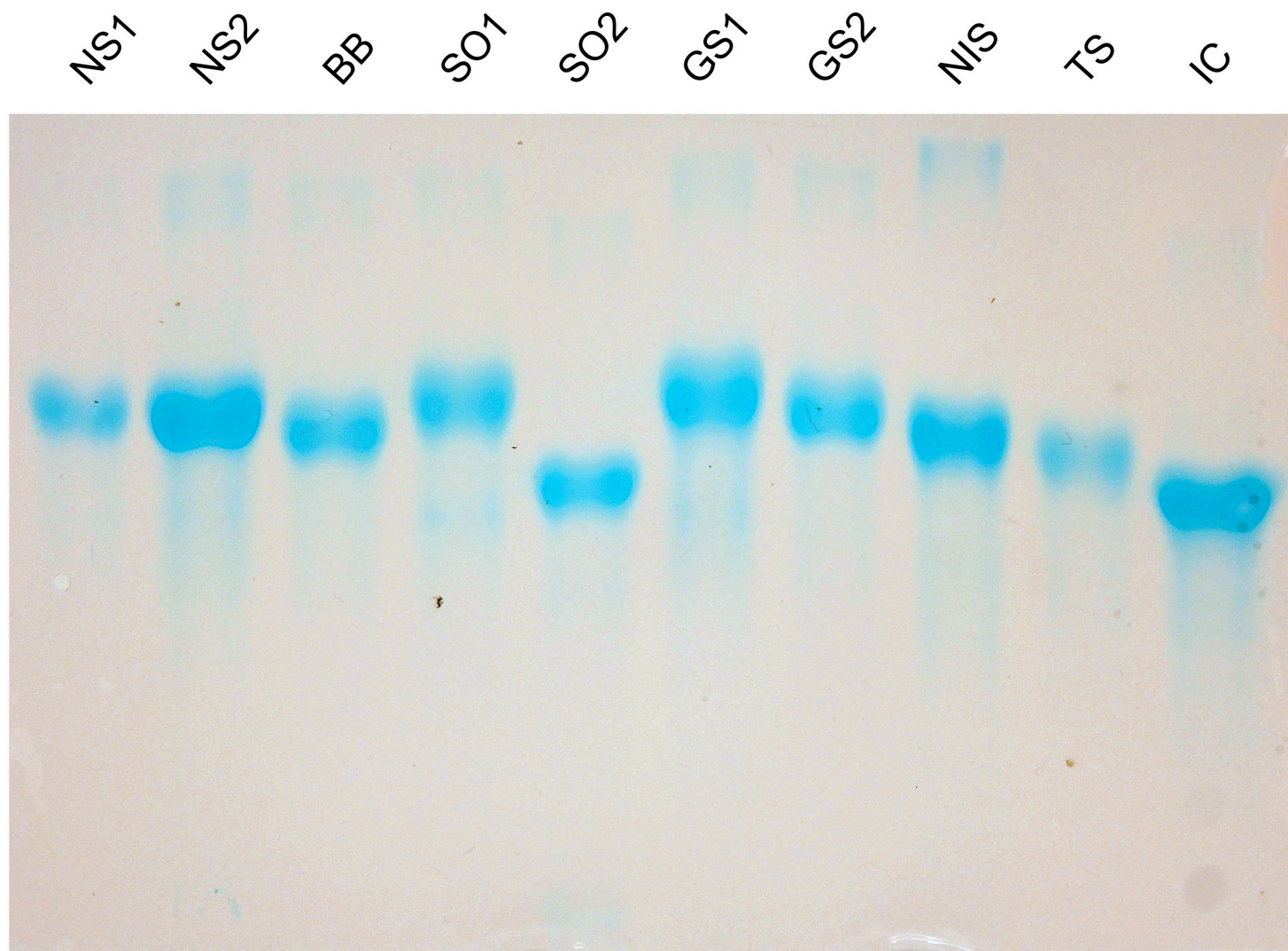


Fig. 5

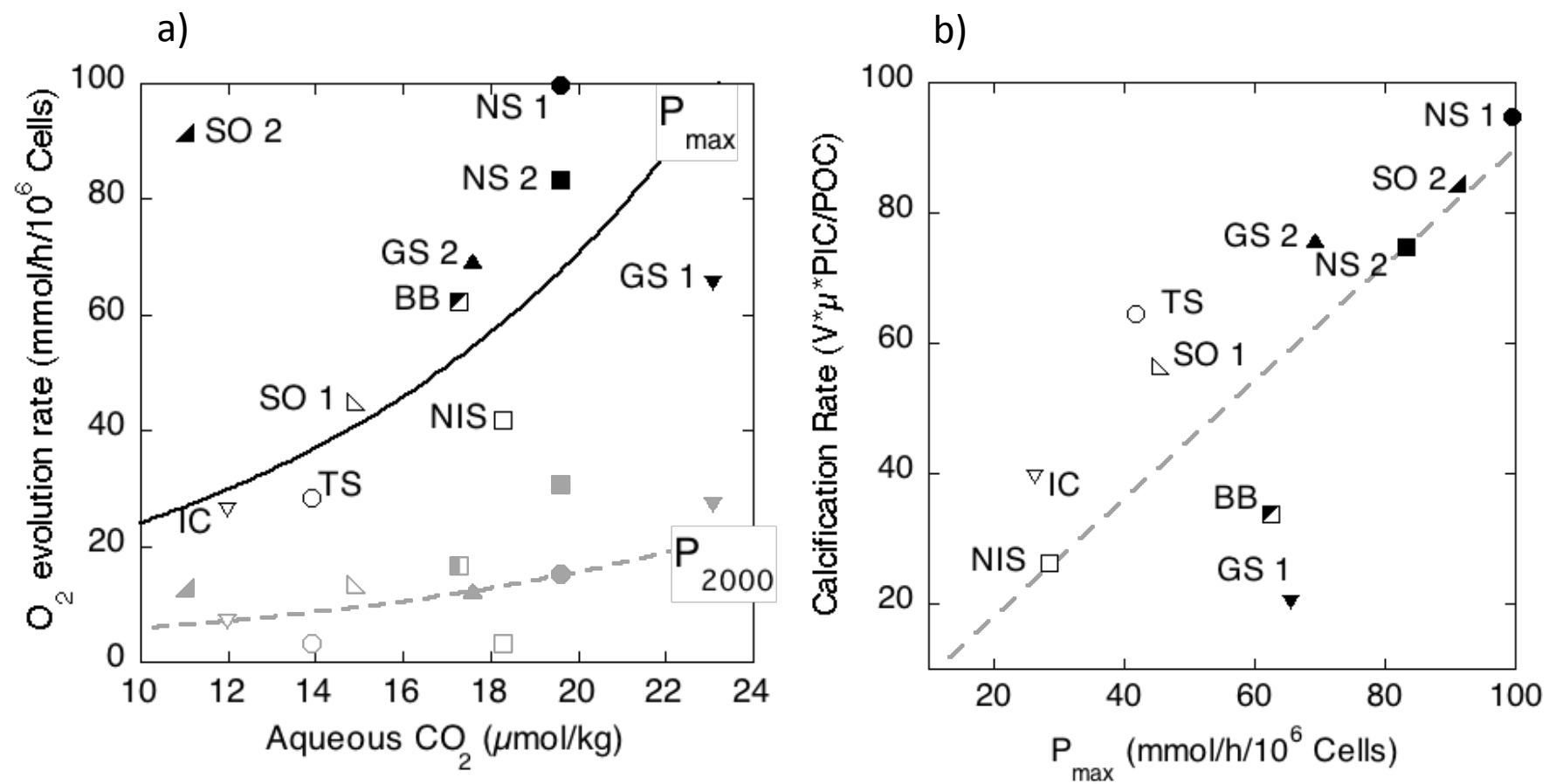


Fig. 6

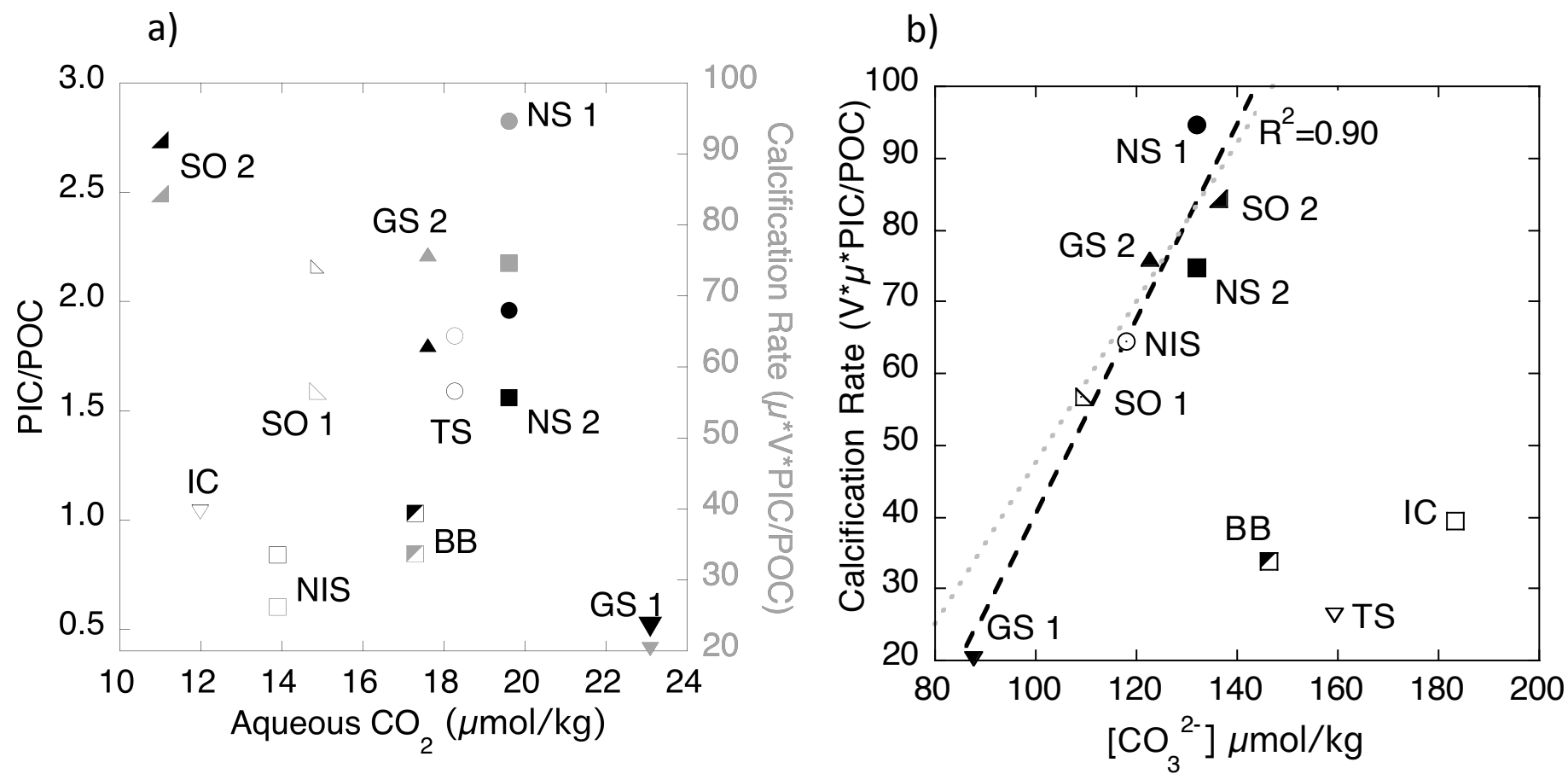


Fig. 7

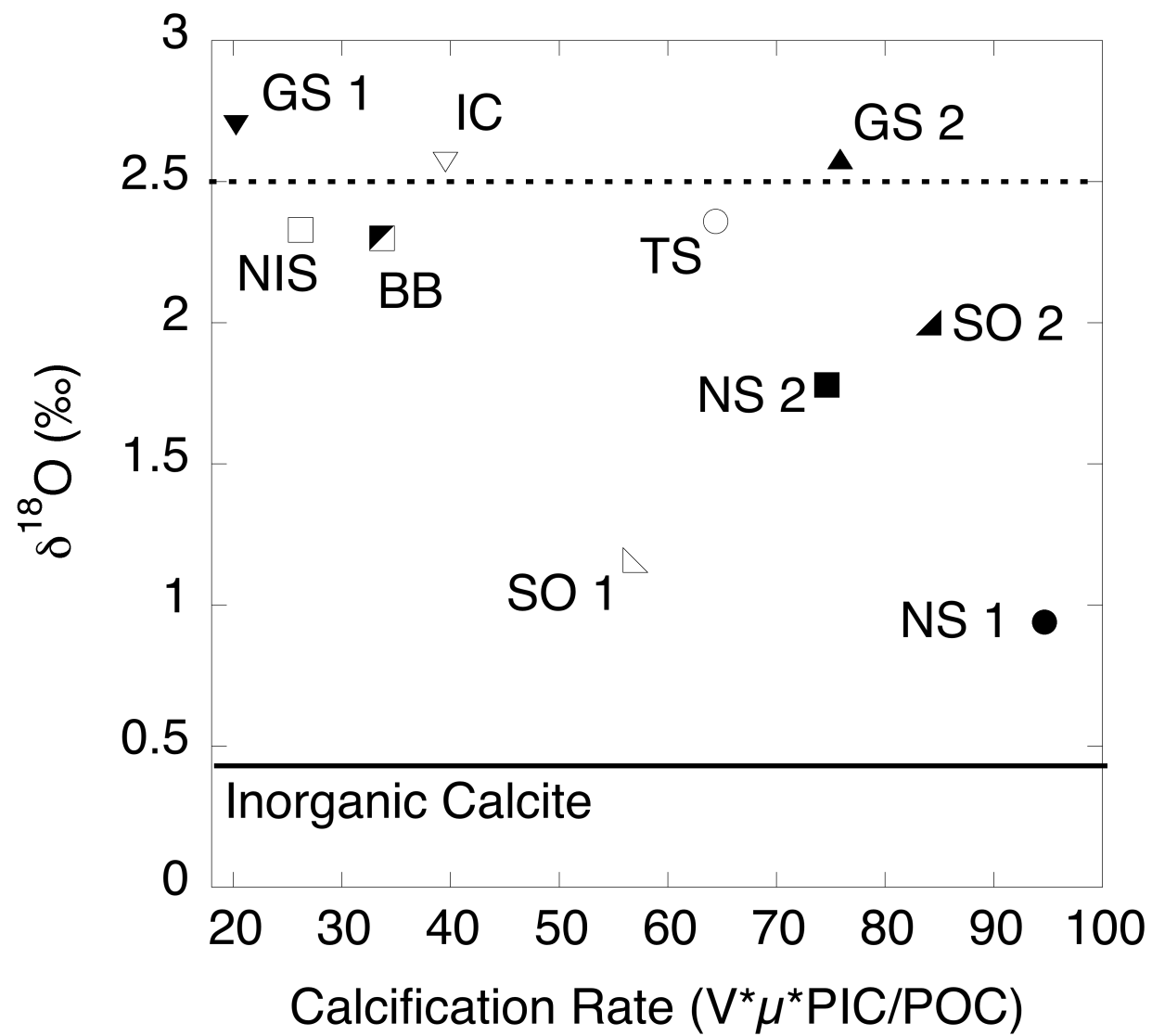


Fig. 8

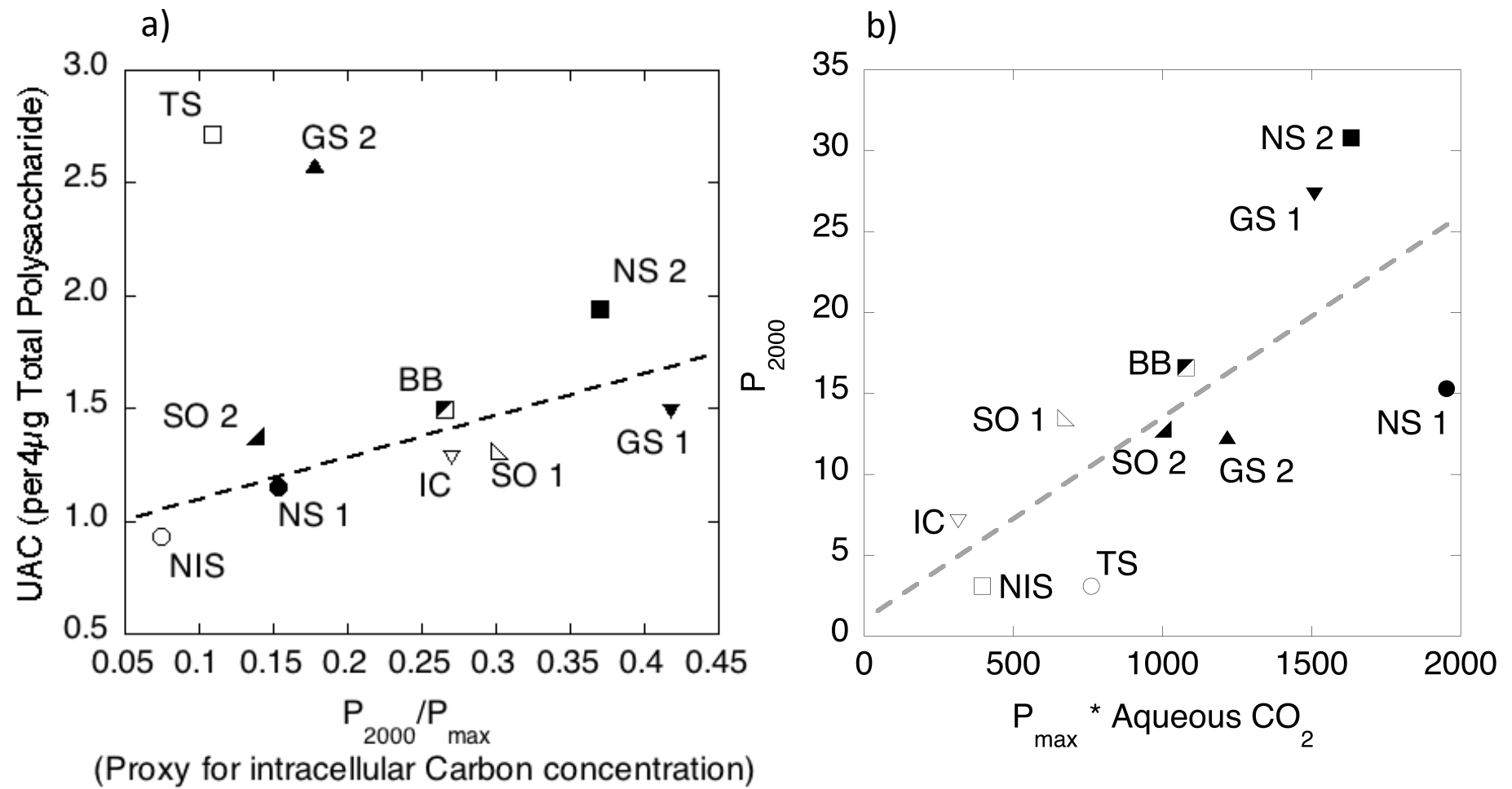


Fig. 9